



Department of Physics, IIT Delhi

**Course Code : PYD561
Semester - II, 2022-23**

High Harmonic Generation in Laser-Plasma Interaction

**Kulwinder Kaur (2021PHS7190)
Harikesh Kushwaha (2021PHS7181)**

Adviser: Prof. Vikrant Saxena

Signature of the first student:

Signature of the second student:

Signature of the adviser:

1 Introduction And Motivation

The study of how light interacts with matter at extremely high-intensity levels, known as Ultra High Light Intensity (UHLI), has garnered significant interest. The main objective is to achieve high-intensity levels, such as the experimental attainment of laser intensities of around $10^{23} W/cm^{-2}$ using the CoReLS petawatt (PW) laser[1], which can provide access to novel physical regimes. At these ultra-high intensities, laser-plasma interactions lead to various nonlinear processes, including the widely studied high harmonic generation[2]. High harmonics have various applications, such as ultrafast quantum information processing, attosecond sources, and all-optical mapping of the electronic band structure. One method of generating high harmonics involves using plasma, which is discussed in this article.

When a laser pulse is incident upon plasma, it reflects if the density of plasma is high, forming PM. Upon reflection from plasma the laser field, because of ponderomotive force, propels a relativistic oscillation of the PM which results in periodic temporal compression of the reflected field. These oscillations result in the generation of high harmonics of the incident laser frequency.[3] Experimental demonstrations have shown the generation of high harmonics up to the 141st order of Nd glass laser[4], 109th order of Ti sapphire laser[5], and 37th order of krypton fluoride laser[6].

To begin, a concise explanation of high harmonic generation is provided, including its occurrence in both gases[7][8][9] and plasma[10][11][12][13][14]. The focus then shifts to the generation of harmonics of an incident laser pulse through interaction with an overdense plasma layer at a step boundary, under the influence of a high-intensity laser pulse. The impact of the laser pulse envelope, super-Gaussian (SG) with different rank p , on the resulting high harmonics is explored. Previously, simulations involving normal laser incidence revealed that only odd harmonics were generated. However, in the present report, various polarization and oblique incidences of laser light are simulated, resulting in the generation of both odd and even harmonics. For this, fully relativistic particle-in-cell simulations are performed using *EPOCH*[15].

2 Theoretical Background

High harmonic generation (HHG) is an optical phenomenon that involves nonlinear processes wherein laser light frequency is converted into multiple integer multiples. When atoms and molecules are exposed to intense laser fields, typically in the near-infrared range, harmonics of extremely high orders are produced.[9] We will start by defining some plasma parameters. Then we will give a brief overview of the theory of HHG in gases, followed by a detailed discussion of HHG in plasma.

2.1 Plasma Parameters

2.1.1 Underdense and Overdense Plasma

Plasma frequency of a plasma with density n_p is given by[16]

$$\omega_p = \sqrt{\frac{n_p e^2}{\epsilon_0 m_e}} \quad (1)$$

Let the frequency of the incident laser pulse be ω_l . Now, if $\omega_l > \omega_p$, the plasma is called *underdense*. In this case, the plasma is transparent to the laser pulse. On the other hand, if $\omega_l < \omega_p$, the plasma is called *overdense*. In this case, the laser can not penetrate the plasma and is reflected back. The case $\omega_l = \omega_p$ corresponds to critical plasma and density in this case is called *critical density* n_c . Using Equation 1 gives;

$$n_c = \frac{\epsilon_0 m_e \omega_l^2}{e^2} \quad (2)$$

2.1.2 Relativistic Laser Pulse

For a laser of frequency ω_l and electric field amplitude E_0 , the laser vector potential is defined as

$$a_0 = \frac{e E_0}{m \omega_l c} \quad (3)$$

A laser is called relativistic if $a_0 \geq 1$. In this situation, the intensity of laser becomes very high and it starts to drive the charged particle it interacts with by relativistic speeds.

2.2 HHG in Gases

HHG phenomena take place when gases are subjected to the influence of an intense laser pulse. The interaction leads to three different types of ionization, which are dependent on the intensity and frequency of the light. If the photon's energy is equal to or greater than the ionization potential of the atom, photon ionization will occur. On the other hand, if the laser's energy is lower than the ionization potential of the atom, multiphoton ionization and tunneling ionization will occur instead. The determination of multiphoton and tunneling ionization depends on the atomic ionization potential I_p , the laser frequency ω , and the amplitude of the laser field strength F . In the multiphoton limit, the rate of ionization follows a power law, whereas in the tunneling limit, it increases exponentially as the field strength increases. The adiabaticity parameter, given by

$$\gamma = \Omega \sqrt{2I_p/F} \quad (4)$$

determines the boundary between multiphoton and tunneling ionization, with high values corresponding to multiphoton ionization and low values to tunneling ionization. To be precise, $\gamma^2 \gg 1$ corresponds to multiphoton ionization and $\gamma^2 \ll 1$ to tunneling ionization.[8]

2.2.1 Three Step Model

In three-step model, we treat the motion of electron initially using quantum mechanics. After it tunnel ionizes from the parent atom, we treat its subsequent dynamics classically. The HHG occurs in three steps:

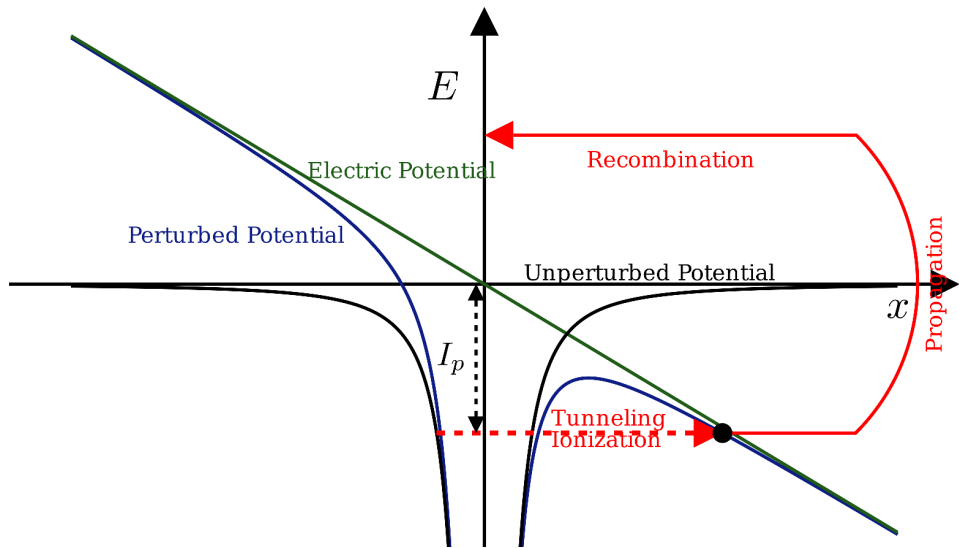


Figure 1: Three steps and fields. The solid black line in the figure shows the binding potential well. The green line is the potential due to the laser field while the solid blue line is the potential created by the instantaneous laser field along with the binding potential well.

All the illustrations in this sections, if not stated otherwise, are made by the authors using manim[17].

- Tunnel ionization** The laser field, which we have assumed to be linearly polarized along the x -axis, gives a potential in the form of $\hat{V}_L(t) - xF\cos(\omega_L t)$, that is, the potential is proportional to $-x$. This is drawn in figure 1 as the green line. When this potential couples with the original potential well (in the black line), the potential is deformed (the blue line), called barrier suppression. Electron tunnels through this potential well.
- Free propagation in the presence of the field** After tunneling, the electron is considered to have no initial velocity as it enters the vacuum. It then experiences acceleration from the electric field of the laser beam. About half a cycle after being ionized, the electron changes direction and moves back toward the parent nucleus due to the reversal of the electric field's direction. During this process, the electron continues to be accelerated.
- Recollision and recombination** Next, the electron will collide with the nucleus which is the recombination process. During recombination, while the electron returns to its ground state, it can

emit radiation of frequency that are multiple of the laser intensity. This is how high harmonics are generated.

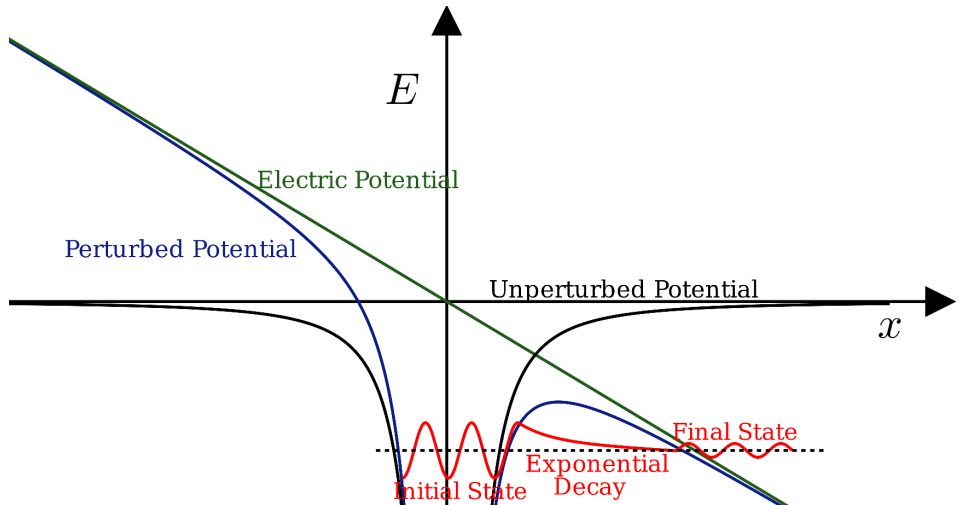


Figure 2: The wave functions of electrons (the red lines). Initially, it is in a potential well. While tunneling, the wave function decay exponentially. After the electron has tunneled through the barrier, it behaves like a free particle with a wave function specified by a smaller amplitude.

2.3 HHG in Plasma

The spectrum from HHG consists of several of integer harmonics of the incident laser pulse (with their intensities decreasing), followed by a plateau, a region, where the harmonic intensity is almost constant over many orders and finally a sharp cutoff. Several of models and theories have been proposed explaining this power law and cutoff. Bezzerides et al.[10] gave the first model way back in 1983. Their model was based on the relativistic equation of motion and hydrodynamics approximation. They found a cutoff frequency as

$$n_{\max}^2 = \frac{n_p}{n_c} \quad (5)$$

where n_p is the plasma density and n_c is the critical density. The authors showed that the main cause of high-harmonic emission is the powerful nonlinear restoring force that arises during resonant absorption in a density profile that is extremely steep. However, this model was not able to explain the plateau region as well as the fact that we get harmonics that are much higher than the cutoff frequency given by Eq. 5.

2.3.1 Oscillating Mirror Model

The concept underlying this model is that the incident laser field induces a periodic oscillation of the plasma mirror surface at relativistic speeds. This oscillating mirror at relativistic speeds results in a periodic Doppler effect on the reflected field, which is responsible for the occurrence of HHG. In this model, it is assumed that the duration of the light pulse is brief enough for the motion of the ions to be disregarded. The ions are considered as a static positive background charge. Additionally, the details of changes in the electron density profile are ignored, and the collective motion of the electrons is represented by the motion of the boundary of the supercritical region. This boundary serves as an effective reflective surface that undergoes oscillatory motion, which is referred to as the oscillating mirror. Using these assumptions, we follow von der Linde et al.[11] to derive the spectrum of HHG. First, we show that the HHG can be understood as a phase modulation due to the moving mirror.

For this, assuming retardation can be neglected for a moment, the phase shift of the reflected wave caused by a sinusoidal displacement of the reflecting surface in the z-direction is affected.

$$s(t) = s_0 \sin(\omega t)$$

is given by

$$\phi(t) = (2\omega_0 s_0/c) \cos \alpha \sin \omega_m t$$

where α is the angle of incidence and ω_m is the mirror frequency (modulation frequency). The reflected wave has the electric field as:

$$E_R \propto e^{-i\omega_0 t} e^{i\phi(t)} = e^{-i\omega_0 t} \sum_{n=-\infty}^{n \rightarrow \infty} J_n(\chi) e^{-in\omega_m t} \quad (6)$$

with $J_n(\xi)$ being the Bessel function of order n and

$$\chi = \frac{2\omega_0 s_0 \cos \alpha}{c} \quad (7)$$

The reflecting surface undergoes periodic motion at a frequency of $2\omega_0$, or a superposition of ω_0 and $2\omega_0$, depending on the polarization and the incidence angle of the incident light. As a result, the modulation frequencies generated by the mirror motion are $\omega_m = \omega_0$ and/or $\omega_m = 2\omega_0$. The crucial point is that this type of modulation gives rise to sidebands representing even and odd harmonics of the fundamental frequency ω_0 . These concepts propose an explanation of high-order harmonic generation from a plasma-vacuum interface as a phase modulation from a reflecting surface that moves periodically.

2.3.1.1 p- and s-Polarization

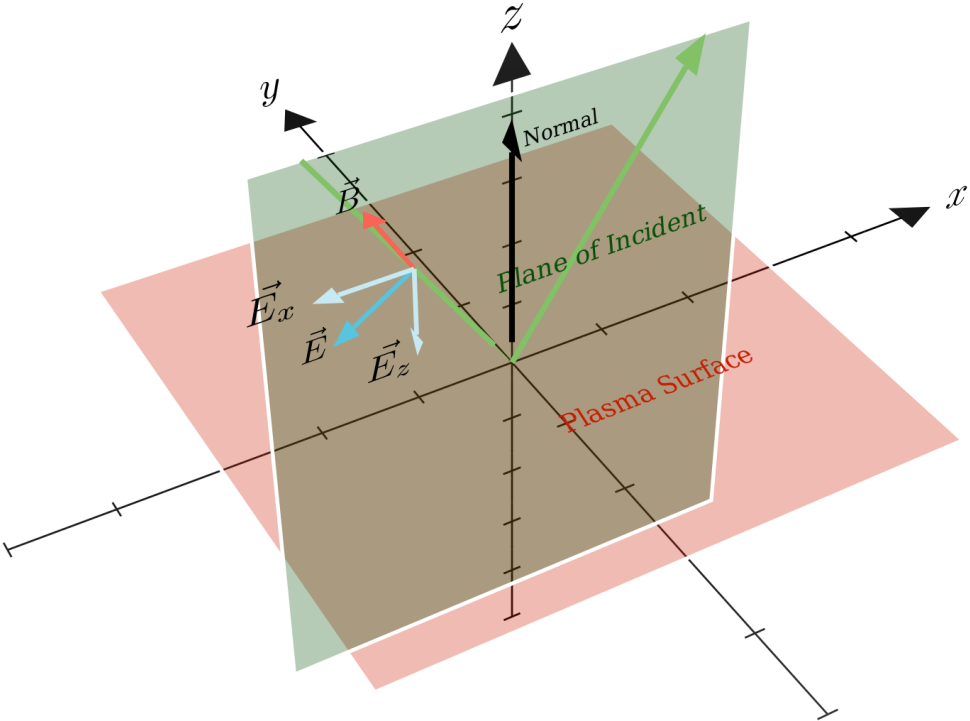


Figure 3: p-polarization. The electric and magnetic fields are parallel and perpendicular, respectively, to the plane of incidence. The motion of the electrons occurs within the plane of incidence.

- **p-Polarized Light:** In this case, the electric and magnetic fields are parallel and perpendicular, respectively, to the plane of incidence. The motion of the electrons occurs within the plane of incidence. The electron boundary is driven at frequencies ω_0 and $2\omega_0$, as both the transverse and longitudinal components of the electron velocity contribute to the motion of the boundary. As a result, both even and odd harmonics with p-polarization are produced in this scenario. Please refer to the Figure 3.
- **s-Polarized Light:** Here, the electric field of the incident light is parallel to the plasma-vacuum interface, while the electrons move in a plane perpendicular to the plane of incidence. In this setup, only the longitudinal component of the electron motion contributes to the mirror motion, while the transverse component is ineffective. Consequently, the mirror motion is driven at a single frequency, $\omega_m = 2\omega_0$. As a result, the reflected light consists of odd harmonics with s-polarization and even harmonics with p-polarization. Please refer to the Figure 4.

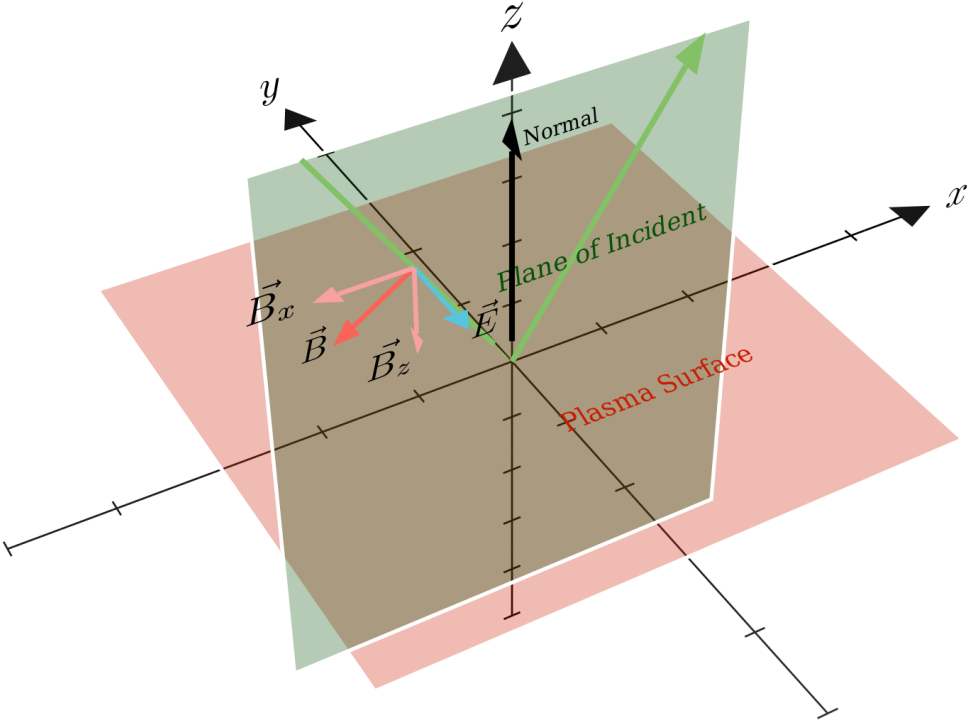


Figure 4: s-polarization. The electric field of the incident light is parallel to the plasma-vacuum interface, while the electrons move in a plane perpendicular to the plane of incidence.

Table 1: Selection Rule for Polarization

	s-polarized Harmonics	p-polarized Harmonics
s-Polarized Fundamental	Odd	Even
p-Polarized Fundamental	None	Odd and Even

2.3.1.2 HHG Spectrum

We chose the coordinate system shown in Fig. 4. The incident light is polarized along the y -axis. The incident light has electric field in the form of:

$$E(t, x, z) = E_0 \exp(-i\omega_0(t - x/c \sin \alpha - z/c \cos \alpha))$$

We assume the surface oscillations to be of the form:

$$s(t) = s_0 \sin(\omega_m(t - x/c \sin \alpha))$$

The maximum displacement of the surface is s_0 is bounded and it is determined by the fact that the velocity must not exceed the speed of light c . For example, for s-polarization, as $\omega_m = 2\omega_0$, we have

$$\begin{aligned} s_0 &< \frac{c}{\omega_0} = \frac{c}{2\omega_0} \\ \therefore \chi &< \cos \alpha \end{aligned}$$

In our analysis, we make the assumption that the reflected wave can be expressed as a plane wave propagating in the direction of specular reflection, given by:

$$E_R = G(u) = G(t - x/\sin \alpha + z/\cos \alpha)$$

Assuming that the reflecting surface is perfectly reflecting, the function $G(u)$ is determined by the requirement that the total field must be zero at the reflecting surface $z = s(t, x)$. This condition can be expressed as:

$$E(t, x, s(t, x)) + E_R(t, x, s(t, x)) = 0 \quad (8)$$

We observe that both the sides of the Eq. 8 are function only of $\xi = t - x/c \sin \alpha$. The spectrum of the reflected wave can be obtained by using the Fourier transform of $G(u)$:

$$G(\omega) = \int_{-\infty}^{\infty} G(u) e^{-i\omega u} du$$

where $u = \xi - s_0/c \cos \alpha \sin(\omega_m \xi)$ Integrating, this comes out to be:

$$G(\omega) = -2\pi E_0 \sum_{-\infty}^{+\infty} \frac{1}{1 + n\omega_m/2\omega_0} \times J_n((1 + n\omega_m/2\omega_0)\xi) \delta(\omega - \omega_0 - n\omega_m) \quad (9)$$

with J_n being the the Bessel function of order n.

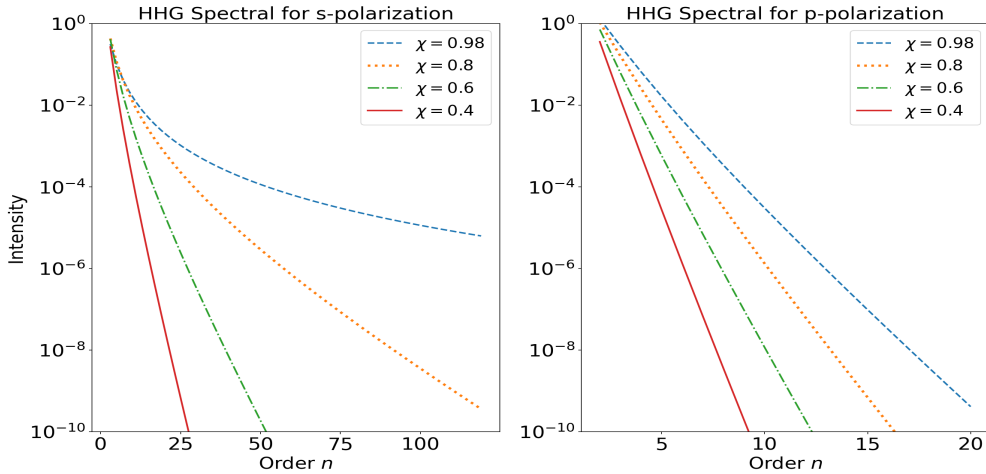


Figure 5: HHG spectrum for s and p polarization. The amplitudes of HHG is decreasing more rapidly for p-polarization than s-polarization

For an s-polarization we have, $\omega_m = 2\omega_0$ and hence equation 9 reduces to:

$$S((2n+1)\omega_0) = (\pi E_0)^2 \left(\frac{J_n((n+1)\xi)}{(n+1)} - \frac{J_{n+1}(n\xi)}{(n)} \right)^2 \quad (10)$$

For a p-polarization:

$$S(n\omega_0) = (\pi E_0)^2 \left(\frac{J_{n-1}(\frac{1}{2}(n+1)\xi)}{\frac{1}{2}(n+1)} - \frac{J_{n+1}\frac{1}{2}((n-1)\xi)}{\frac{1}{2}(n-1)} \right)^2 \quad (11)$$

A plot of the spectra is shown in figure 5.

2.3.2 Universal Spectra

The *ideal mirror* assumptions made by von der Linde et al.[11] are not held in practice. In fact, an ideal mirror is not physically possible. Gordienko et al.[14] showed that it is not necessary to assume a form of plasma surface oscillation if the goal is just to get the cutoff and power law of the HHG spectrum. Assuming only the boundary condition equation 8 and the periodicity of the surface motion, they found the following results which are valid for any type of plasma surface motion:

1. The power law for monochromatic wave

$$I_n \propto 1/n^{5/2} \quad (12)$$

2. The power law for broadband wave

$$I_n \propto 1/n^{5/2}$$

3. The cutoff

$$n_c \propto 4\gamma_{\max}^2 \quad (13)$$

3 Methodology

The present report uses *EPOCH*[15], which is a fully relativistic, 3D, parallelized implementation of the particle-in-cell algorithm.

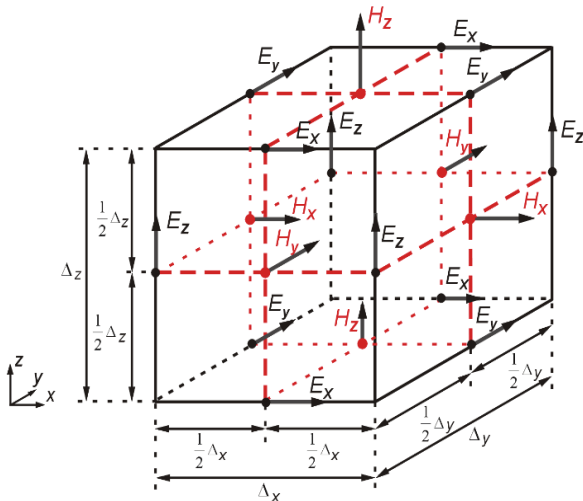
3.1 PIC Approach

The particle-in-cell (PIC) method is a numerical technique used in plasma physics to simulate the behavior of a group of particles interacting through both external and self-induced electromagnetic fields. The simulation is carried out on a spatial grid that describes the fields, while the particles move continuously through space. The motion of both the particles and the fields are solved simultaneously. Since each particle interacts only with the grid points of the cell it is located in, the simulation requires less computational effort. [18]

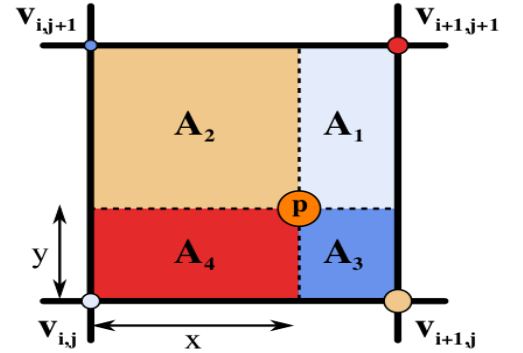
In PIC, the plasma is represented by collection of particles, macro particle, with same charge to mass ratio. The system is discretised parallel to the boundaries forming a grid (mesh). The particles are free to move anywhere inside the system boundaries, however, the continuous electromagnetic field is replaced by discrete values assigned only to the mesh points.

The arrangement of the fields is called the Yee cell. Since the charge density is defined on the corners, the central difference places the electric fields at the edges. Meanwhile, the magnetic fields are located on the face. After the initial condition is given, PIC start by calculating the charge density (ρ) at grid points from nearby charged particles. The charge of each particle is distributed among the grid points using a weighting algorithm. Usually, a bilinear interpolation is used where the charge on the grid is determined using the subarea of the opposite vertex.

In the PIC method, after setting the initial conditions, the next step is to compute the charge density (ρ) at each grid point by gathering the contribution from nearby charged particles. The charge of each particle is distributed among the grid points using a weighting algorithm. Usually, a bilinear interpolation is used where the charge on the grid is determined using the subarea of the opposite vertex.



Update of \mathbf{E} and \mathbf{B} is done by Yee algorithm. The advancement of \mathbf{E} from step n to $n + 1$ is done via central differencing using \mathbf{B} at $n + 1/2$. While, the advancement of \mathbf{B} from step $n - 1/2$ to $n + 1/2$ is done via central differencing using \mathbf{E} and the current density (\mathbf{J}) at step n . Finally, the updated electric and magnetic fields are used to forward velocity for step $n - 1/2$ to $n + 1/2$ and velocity at step $n + 1/2$ is used to forward position for step n to $n + 1$. The charge and hence the current density is updated using this newly updated position which in turn updates magnetic field and the cycle continues. The fact that the velocity (\mathbf{B}) at half step is used to forward position (\mathbf{E}) at full step and vice versa makes this update rule leap-frog



The Yee cell is a staggered grid arrangement used in (PIC) simulations to determine the positions of electric and magnetic field nodes. In this scheme, the electric field components are located at the faces of the cubic cell, while the magnetic field components are located at the edges of the cell. This arrangement ensures accurate and stable time integration of the fields in PIC simulations, making it a widely used scheme in simulating electromagnetic phenomena in plasmas and other complex systems.

method.

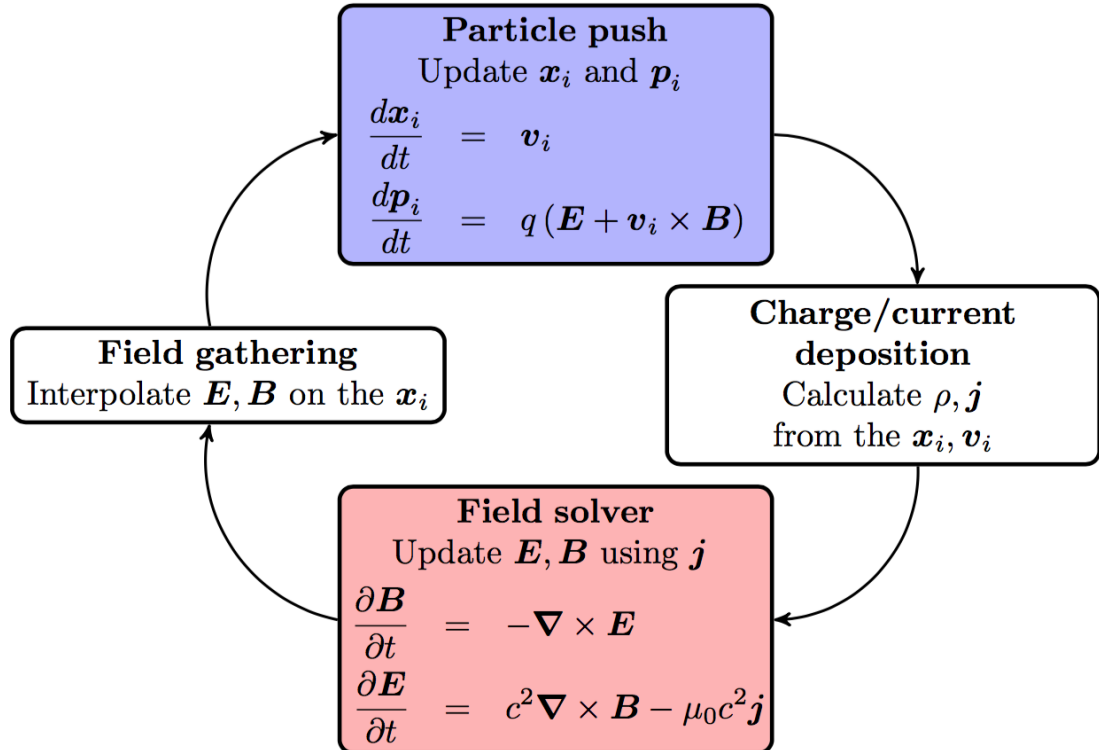


Figure 6: The four steps of a PIC cycle.

The velocity is updated with Boris method. First, a half-step acceleration is performed in the electric field direction, followed by full rotation in magnetic field and finally, another half-step acceleration is performed in the electric field direction.

3.2 Simulation Setup

The present report includes two types of simulations: first, we use a normally incident laser pulse to study the effect of various laser and plasma parameters on generated HHG. Secondly, we have performed some simulations to study the oblique incidence and different polarization.

3.2.1 For Normal Incident

Before, going to the main study, we have performed some preliminary simulations to study how relativistic and non-relativistic laser interact with overdense and underdense plasma. After this, the effect of various laser and plasma parameters on generated HHG are studied. The simulation setup for both simulations is given below.

3.2.1.1 Simulation Setup for Preliminary Study

The simulation box extends for $20\lambda_l$ (from $-10\lambda_l$ to $10\lambda_l$), where λ_l is the laser wavelength and has total 1000 cells, i.e., 50 cells per wavelength. The plasma is placed at $x = 0$ and with a thickness of λ_l . Number of particles per cell are 100. The plasma density n_p is defined in terms of the critical density n_c and is varied from 0.1 to 10. The vector potential a_0 of the laser pulse is also varied as 0.1, 1.0 and 10 for each set of plasma density. The laser envelope is used for this simulation is sine-squared, see equation 14. Where T is the pulse duration here taken as $T = 10\tau$ with $\tau = 2\pi/\omega_l$ is the time of one laser cycle. The simulation is performed for $t = 20\tau$.

3.2.1.2 Simulation Setup for HHG Study

The simulation box extends for $40\lambda_l$ (from $-20\lambda_l$ to $20\lambda_l$), where λ_l is the laser wavelength taken as $1\mu m$ and has a total of 16000 cells, i.e., 400 cells per wavelength. The plasma is placed at $x = 0$ and with a thickness of λ_l . The number of particles per cell is 100. The pulse duration is $T = 20\tau$ and the simulation is run till $T_{end} = 40\tau$. Here τ is the time period of the laser pulse. We have studied effects of different laser envelopes that are given below:

1. Sine Squared

$$P(t) = \begin{cases} \sin^2(\pi t/T) & \text{for } 0 \leq t \leq T \\ 0 & \text{otherwise} \end{cases} \quad (14)$$

2. Gaussian

$$P(t) = \begin{cases} e^{-\frac{(t-T/2)^2}{2(0.2T)^2}} & \text{for } 0 \leq t \leq T \\ 0 & \text{otherwise} \end{cases} \quad (15)$$

3. Triangular

$$P(t) = 2 \times \begin{cases} t/T & \text{for } 0 \leq t \leq T/2 \\ 1 - t/T & \text{for } T/2 \leq t \leq T \\ 0 & \text{otherwise} \end{cases} \quad (16)$$

4. Super-Gaussian

$$P(t) = \begin{cases} e^{-\frac{(t-T/2)^p}{2(0.2T)^p}} & \text{for } 0 \leq t \leq T \\ 0 & \text{otherwise} \end{cases} \quad (17)$$

Here T is the pulse duration and t is the time. The pulse duration is taken as $T = 20\tau$. p is the power of the SG envelope. We also studied the effect of power of SG envelope on generated HHG.

3.2.2 For Oblique Incident

To report uses only a 1D simulation for oblique incidence. This is accommodated by following Bourdier transformation[19], where simulations are performed in a frame which is moving in such a way that the light is normally incident. (See figure 7)

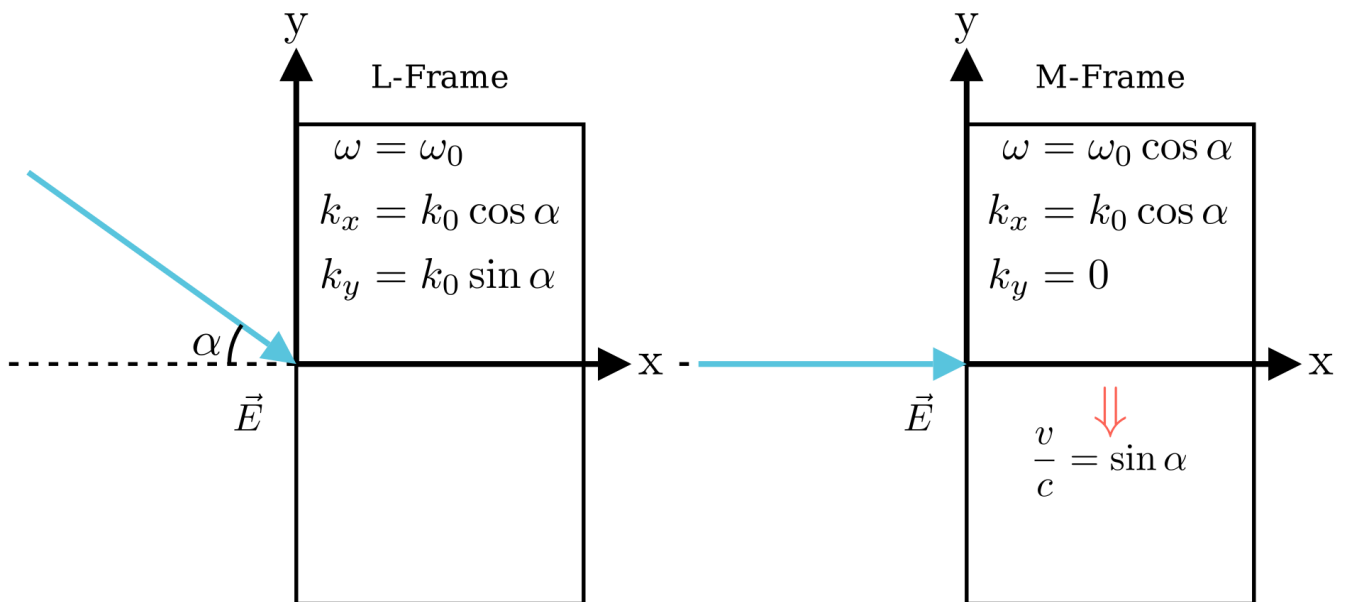


Figure 7: L is the lab frame and M is the moving frame. Simulations are done in the M-frame and then they are transformed back to the L-Frame

3.2.2.1 Bourdier transformation

For this, we make a Lorentz transformation from the laboratory frame L to frame M, moving with a velocity of $\mathbf{v}_M = c \sin \alpha \hat{y}$. As the frame is moving in y direction and the speed is $c \sin \alpha$, the incident pulse is normal to the surface in the M-frame as illustrated in Figure 7. This means that the plasma must be moving with a velocity of $-\mathbf{v}_f$. The frequency ω_0 and the wave vector \mathbf{k}_0 changes so that the speed of light is the same. The transformations of these are in figure 7.

The electric and magnetic field also changes. For p-polarization, the transformation equations are:

$$\begin{aligned}\mathbf{E}_L &= E_0(-\sin \alpha \hat{x} + \cos \alpha \hat{y}) \\ \mathbf{E}_M &= E_0 \cos \alpha \hat{y} \\ c\mathbf{B}_L &= E_0 \hat{z} \\ c\mathbf{B}_M &= E_0 \cos \alpha \hat{z}\end{aligned}\tag{18}$$

While for s-polarization:

$$\begin{aligned}\mathbf{E}_L &= E_0 \hat{z} \\ \mathbf{E}_M &= E_0 \cos \alpha \hat{z} \\ c\mathbf{B}_L &= E_0(\sin \alpha \hat{x} - \cos \alpha \hat{y}) \\ c\mathbf{B}_M &= -E_0 \cos \alpha \hat{y}\end{aligned}\tag{19}$$

Note that the amplitudes of the field are scaled down by a factor of $\cos \alpha$ and hence intensity also decreases. However, the normalized vector potential $a_0 = eE_0/m\omega_0 c$ remains invariant. The density becomes $n_M = n_0 / \cos \alpha$. A summary of these transformations is given in the table below:

Table 2: Transformation Equations

Quantity	L-Frame	M-Frame
ω	ω_l	$\omega_l \cos \alpha$
λ	λ_l	$\lambda_l / \cos \alpha$
n	n_0	$n_0 / \cos \alpha$
\mathbf{E} (p-polarized)	$E_0(-\sin \alpha \hat{x} + \cos \alpha \hat{y})$	$E_0 \cos \alpha \hat{y}$
\mathbf{E} (s-polarized)	$E_0 \hat{z}$	$E_0 \cos \alpha \hat{z}$
\mathbf{B} (p-polarized)	$E_0 \hat{z}$	$E_0 \cos \alpha \hat{z}$
\mathbf{B} (s-polarized)	$E_0(\sin \alpha \hat{x} - \cos \alpha \hat{y})$	$-E_0 \cos \alpha \hat{y}$

3.2.2.2 Simulation Setup for Oblique Incident

The simulation box extends for $40\lambda_l$ (from $-20\lambda_l$ to $20\lambda_l$), where λ_l is the laser wavelength taken as $1\mu m$ and has a total of 16000 cells, i.e., 400 cells per wavelength. The plasma is placed at $x = 0$ and with a thickness of λ_l . The number of particles per cell is 100. The pulse duration is $T = 20\tau$ and the simulation is run till $T_{end} = 40\tau$

4 Results and Discussion

All the plots in this sections are made by the authors using matplotlib[20]. We would like to acknowledge NumPy[21] and SciPy[22] for providing the necessary tools to visualize, preprocess and derive meaningful insights from the simulations.

4.1 Normal incidence

In this section, we will discuss the results of the simulations for normal incidence. A number of simulations are performed to study the different laser and plasma parameters on the generated HHG and the plasma oscillations. We will first start by discussing how overdense and underdense plasma behaves in presence of relativistic and non-relativistic laser pulse.

4.1.1 Preliminary Analysis

The goal is to study the transmittance and reflectance of the laser pulse in underdense and overdense plasma for relativistic and non-relativistic case. For this, we define a term calling it the *reflectance* as:

$$R = \frac{E_b^2 - E_a^2}{E_b^2} \quad (20)$$

where E_b is the sum of y component of the electric field at a node before the plasma starts and E_a is the sum of y component of the electric field at a node where plasma just ends. This way, the above relation gives a indication of the ratio of the intensity passing through the plasma to the intensity getting reflected.

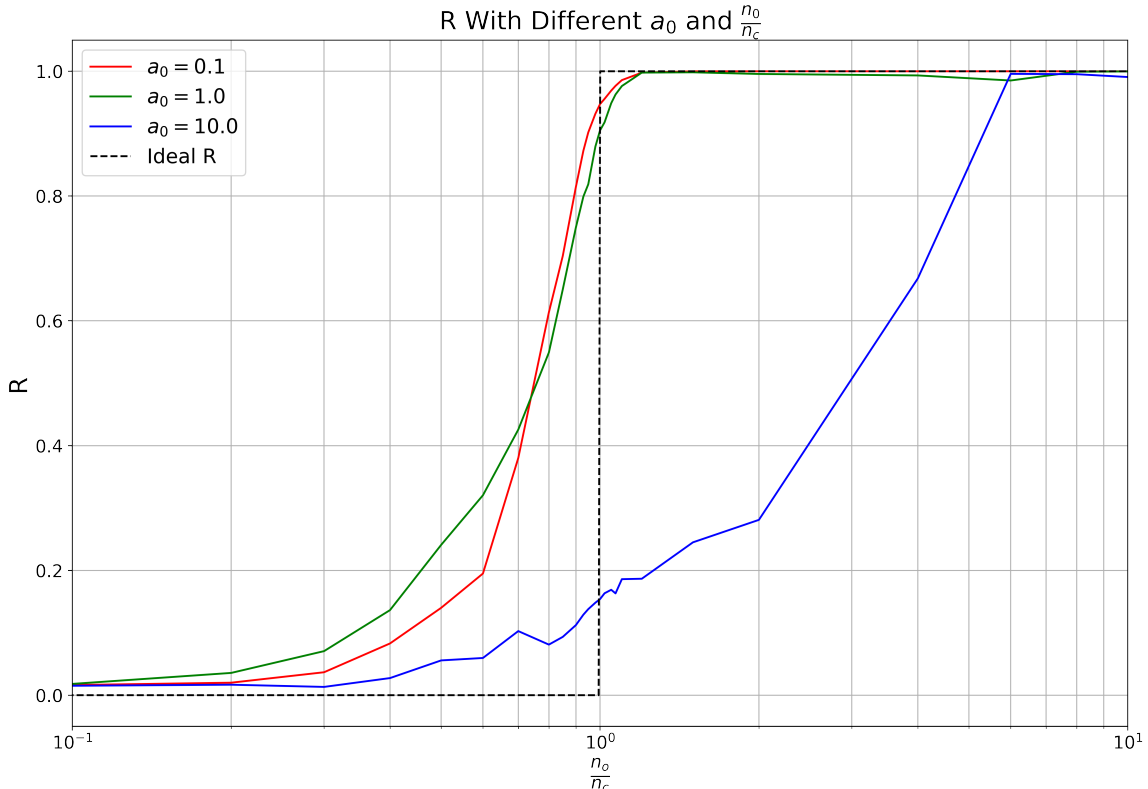


Figure 8: Plot of reflectance (see 20) with different ratio of n_c and n_0 and vector potential a_0 . Black dotted line represents the ideal behavior.

The ideal curve for the interaction of laser pulse with underdense and overdense plasma is also shown in the figure with black dotted line. Ideally, when the ratio $r = \frac{n_0}{n_c}$ becomes 1, the reflectance also becomes 1. However, when the laser becomes relativistic for $a_0 \geq 1$, the particles inside plasma starts to oscillate with relativistic velocity, gaining mass. This results in change in the plasma frequency and hence the laser does not get reflected even for density greater than the critical density corresponding to the non-relativistic case. So, there is a shift in the critical density due to relativistic laser pulse.

Next, the plot of these oscillation of plasma surface with time is also shown for different values of vector potential (Figure 9). The plasma density is taken to be critical density, i.e., $r = 1$. The laser pulse, after interacting with electrons, makes them oscillate. If the pulse becomes relativistic, the oscillations becomes strong and hence the plasma surface oscillates with relativistic velocity.

This completes the preliminary analysis of laser-plasma interaction. In the next section will discuss about effects of various laser and plasma parameters on the HHG generation.

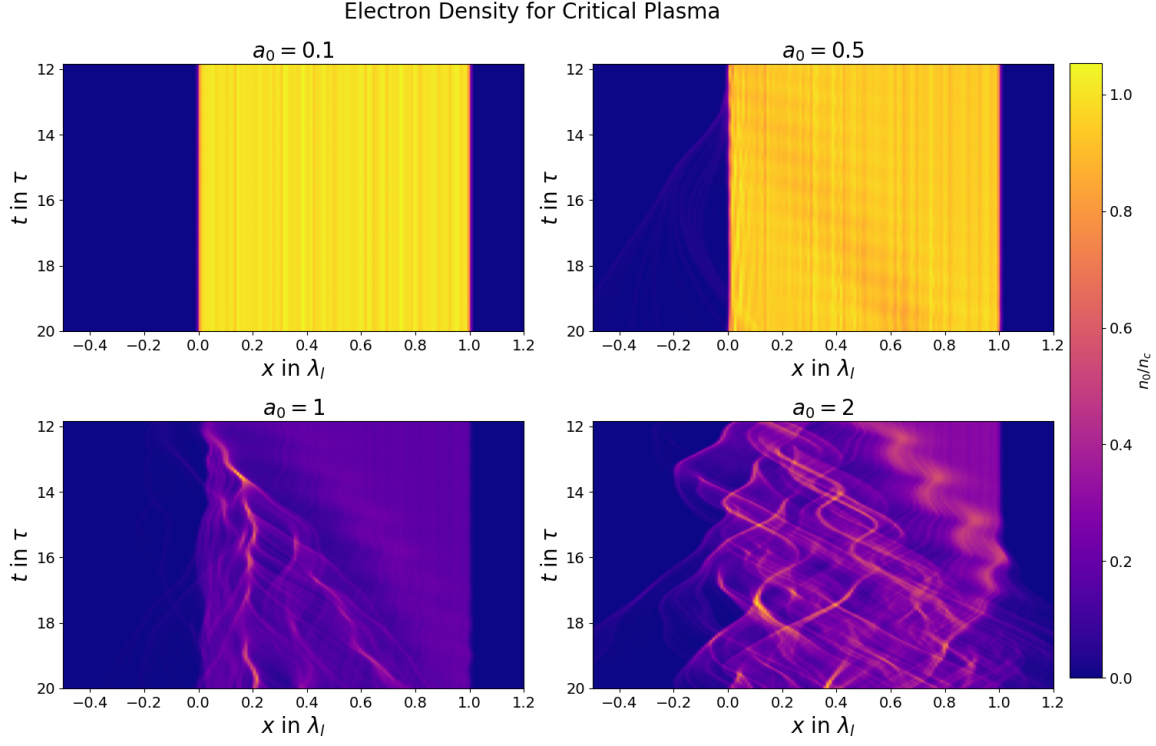


Figure 9: The effect of relativistic laser pulse on the plasma density oscillations. For $a_0 = 0.1$, the oscillation is very weak. As a_0 increases, the oscillation becomes stronger.

4.1.2 Effects On Generated HHG

This section shows results which were obtained by varying the laser and plasma parameters.

4.1.2.1 Effect of Plasma Density

No significant effect of plasma density on generation of high harmonics is observed. However, a resonance is observed at plasma density of $4n_c$ giving more harmonics at that density (See figure 10). This resonance is because the plasma frequency is equal to the frequency of the driving ponderomotive force. (Since $F \propto (1 - \cos 2\omega t)$)

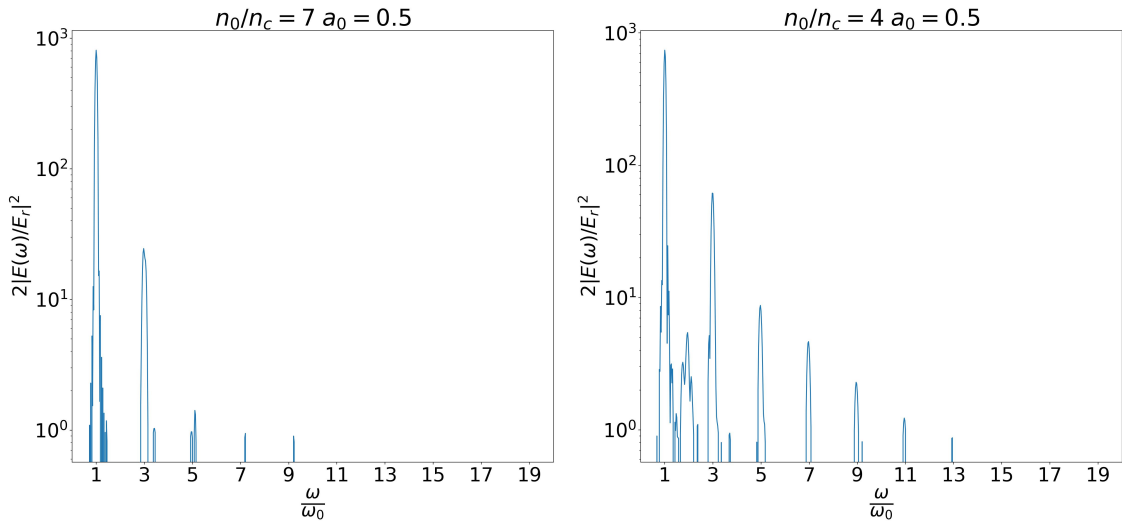


Figure 10: Resonance at $n = 4n_c$

4.1.2.2 Effect of Laser Intensity

Increasing the laser intensity increases the number of harmonics generated. The amplitude of the harmonics also increases. The Figure 11 shows the effect of laser intensity on the harmonics generated.

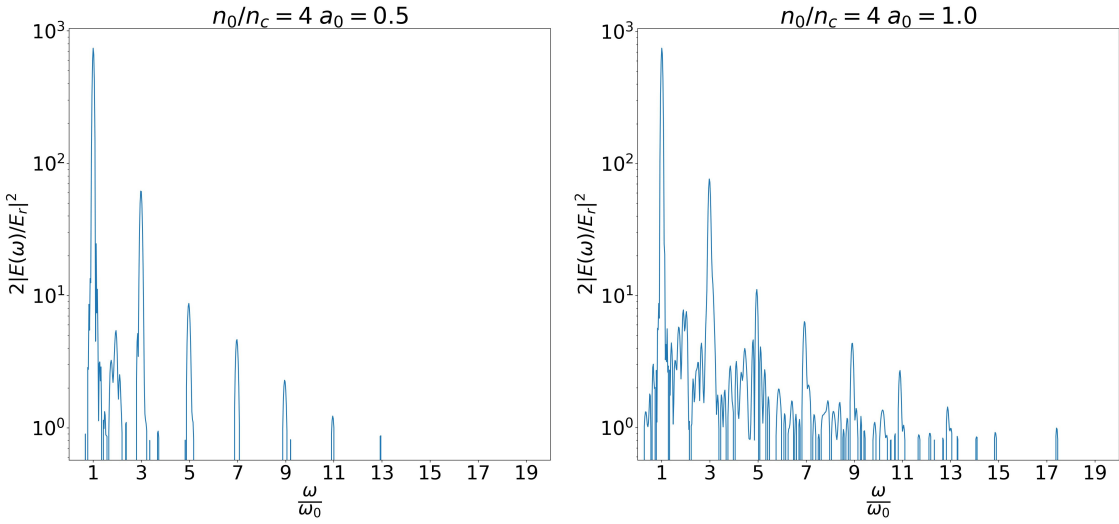


Figure 11: Laser intensity and the harmonics generated.

4.1.2.3 Effect of Laser Envelope

The laser envelope does not seem to have any effect at all. See the Figure 12.

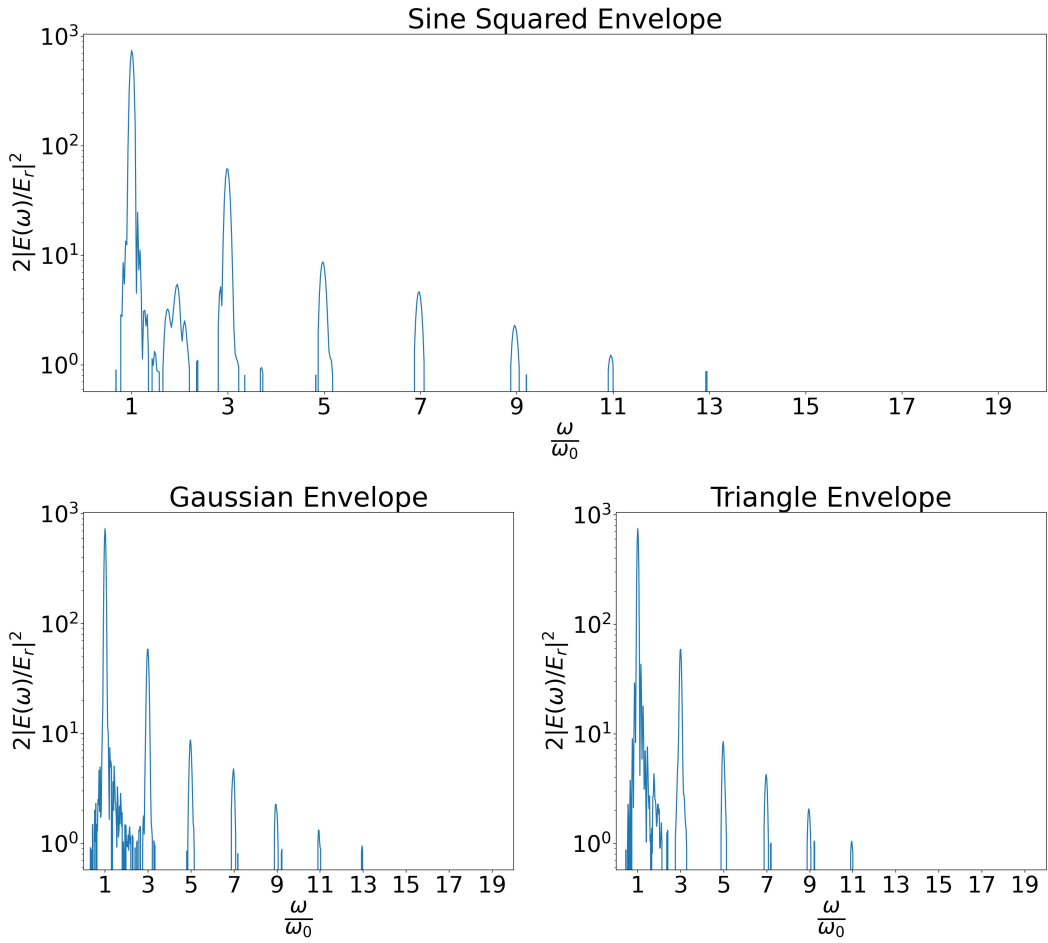


Figure 12: Effect of the laser envelope on the harmonics generated.

4.1.2.4 Effect of Pulse Duration

Increasing the pulse duration increases power within the pulse which then increases the number of harmonics generated. The harmonics also become more pronounced in amplitude. The Figure 13 on shows the effect of the laser pulse duration on the harmonics generated.

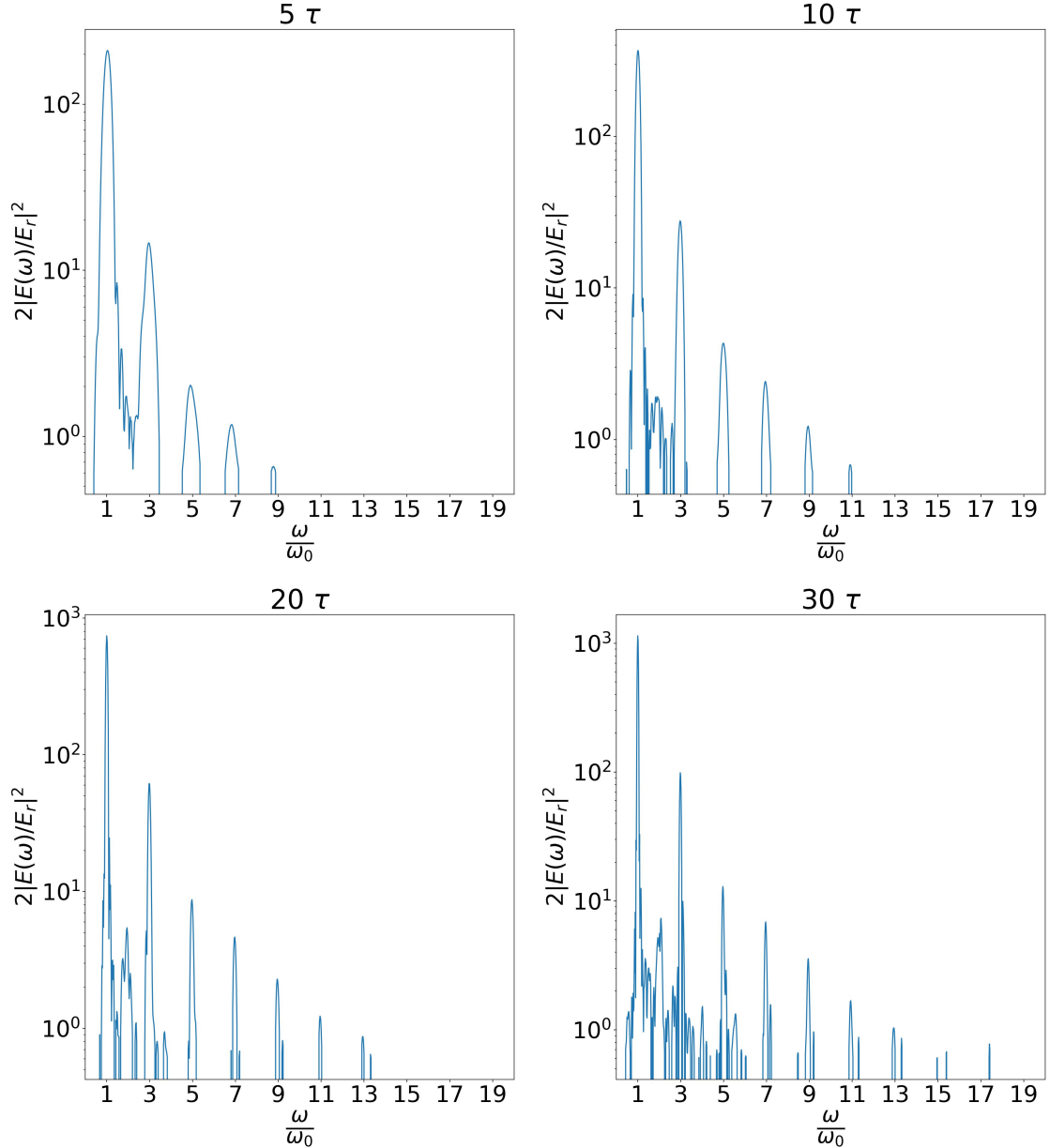


Figure 13: Effect of the laser pulse duration on the harmonics generated.

4.1.2.5 Super-Gaussian Envelope

The SG envelope, given by equation 17 has a different area for different p and hence has different energy for the same given intensity. To mitigate this, the simulation is performed by multiplying the given intensity of the pulse such that the total energy of all the pulses is the same. This is done by taking a reference SG beam (we have used $p = 2$), evaluating its area and then normalizing the intensities of other SG pulses by the ratio of this reference area and the area of the corresponding SG envelope. The spectrum of the HHG generated using laser pulse with SG envelopes with power 2, 4, 6, and 8 are shown in figure 14. It is observed that a small increase in the amplitude is followed by increasing power of the SG envelope.

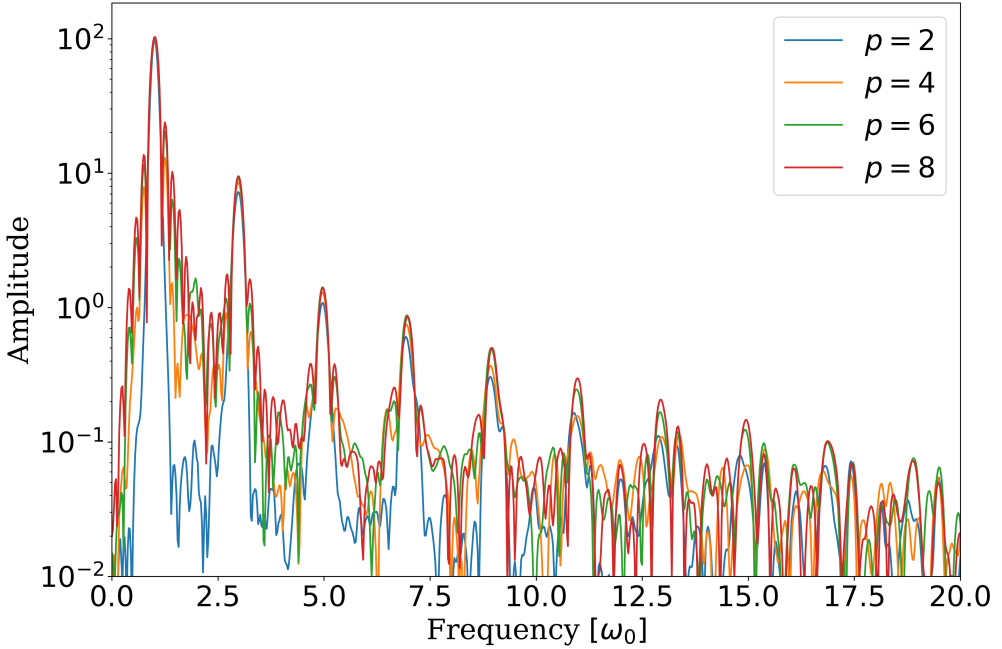


Figure 14: The spectrum of SG envelopes with power 2,4,6, and 8 are shown in a single plot. A small increase in the peak amplitude is observed with increasing power.

4.1.3 The Frequency of Plasma Oscillations

We found out that the frequency of oscillations is even harmonic of the frequency of the incident laser pulse. Furthermore, electrons are oscillating only till they are interacting with the laser field. (See the Figure 15)

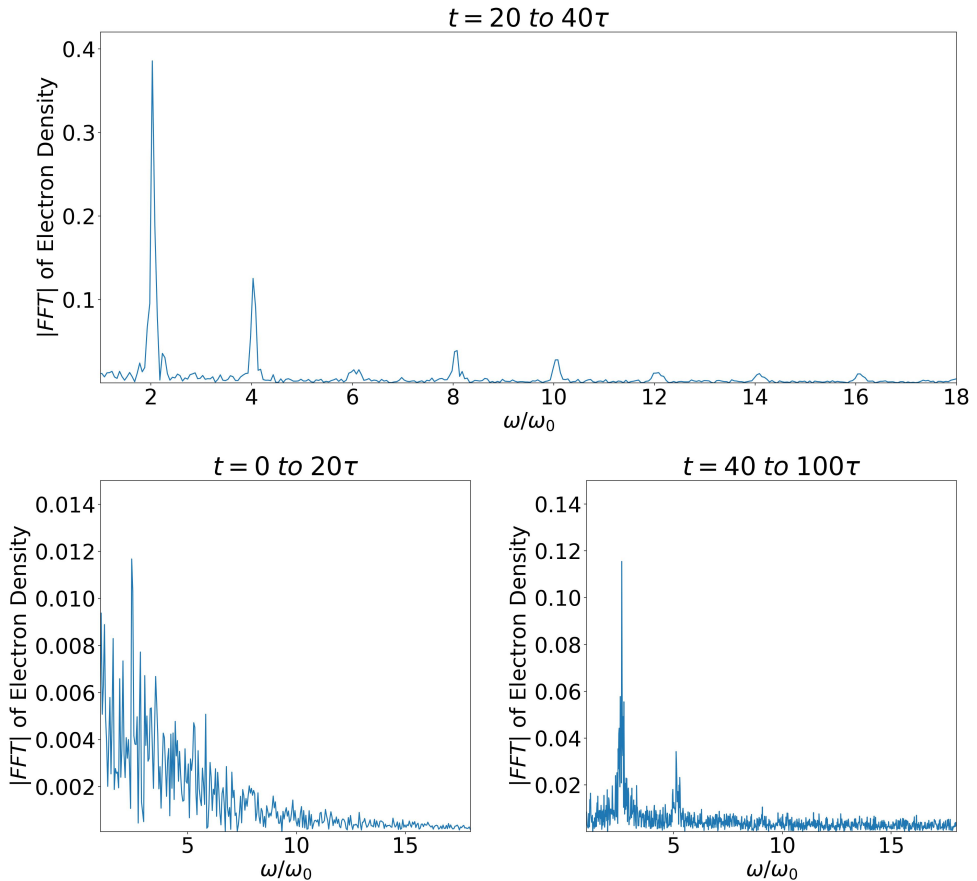


Figure 15: Frequency of electron oscillations during different times

4.2 Oblique Incidence

4.2.1 p-Polarization

Figure 16 shows the spectrum of HHG in the L-frame, when p-polarized light is incident on the plasma. As discussed in section 2.3.1.1 (see the table 1), the spectrum is made up of even and odd p-polarized harmonics. There are no s-polarized harmonics.

4.2.2 s-Polarization

The L-frame spectrum of HHG is depicted in diagram 16, with plasma being exposed to s-polarized light. As explained in section 2.3.1.1 (see the table 1), the spectrum comprises odd s-polarized harmonics and even p-polarized harmonics.

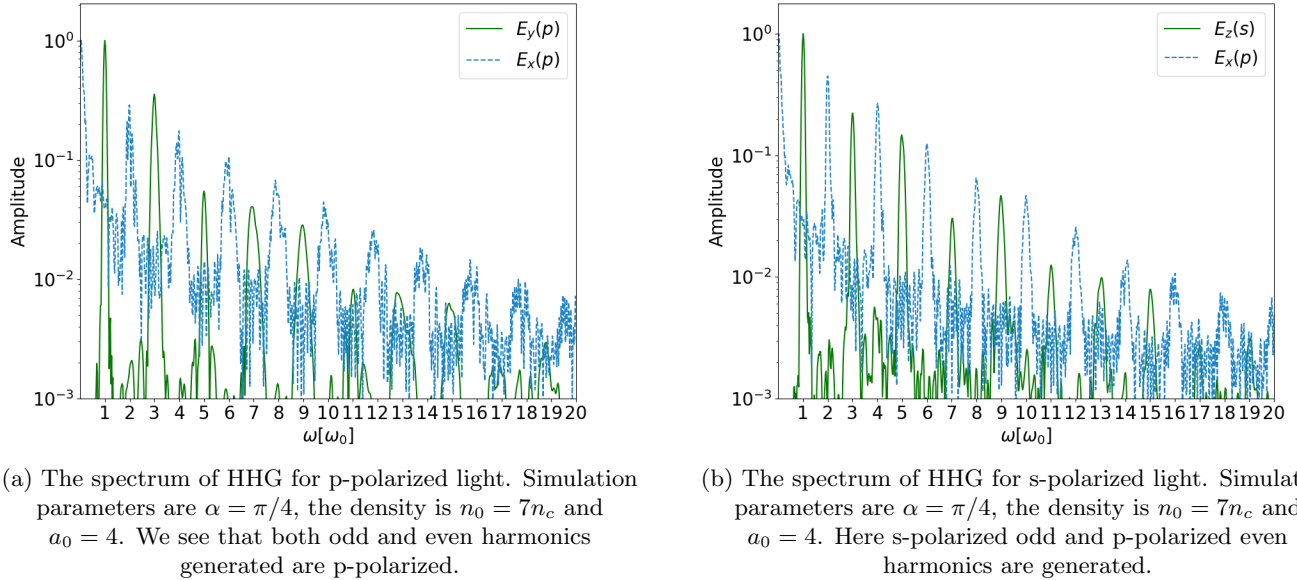


Figure 16: p- and s- polarized light

5 Acknowledgment

We would like to extend our sincerest gratitude to Professor Vikrant Saxena for his unwavering support, patience, motivation, enthusiasm, and invaluable guidance. His mentorship and leadership have been instrumental in the success of this project, and we feel incredibly fortunate to have had the opportunity to work with him.

References

- [1] Jin Woo Yoon et al. “Realization of laser intensity over 1023 W/cm²”. In: *Optica* 8.5 (May 2021), pp. 630–635. DOI: 10.1364/OPTICA.420520. URL: <https://opg.optica.org/optica/abstract.cfm?URI=optica-8-5-630>.
- [2] Henri Vincenti. “Achieving Extreme Light Intensities using Optically Curved Relativistic Plasma Mirrors”. In: *Physical Review Letters* 123.10 (Sept. 2019). DOI: 10.1103/physrevlett.123.105001. URL: <https://doi.org/10.1103/physrevlett.123.105001>.
- [3] R. Lichters, J. Meyer-ter-Vehn, and A. Pukhov. “Short-pulse laser harmonics from oscillating plasma surfaces driven at relativistic intensity”. In: *Physics of Plasmas* 3.9 (1996), pp. 3425–3437. DOI: 10.1063/1.871619. URL: <https://doi.org/10.1063/1.871619>.
- [4] Michael D. Perry and Gerard Mourou. “Terawatt to Petawatt Subpicosecond Lasers”. In: *Science* 264.5161 (1994), pp. 917–924. DOI: 10.1126/science.264.5161.917. URL: <https://www.science.org/doi/10.1126/science.264.5161.917>.
- [5] J. J. Macklin, J. D. Kmetec, and C. L. Gordon. “High-order harmonic generation using intense femtosecond pulses”. In: *Phys. Rev. Lett.* 70 (6 Feb. 1993), pp. 766–769. DOI: 10.1103/PhysRevLett.70.766. URL: <https://link.aps.org/doi/10.1103/PhysRevLett.70.766>.
- [6] S G Preston and J B Watson. “Generation of a harmonic quasi-continuum from beating laser fields”. In: *Journal of Physics B: Atomic, Molecular and Optical Physics* 31.10 (Apr. 1998), p. 2247. DOI: 10.1088/0953-4075/31/10/014. URL: <https://dx.doi.org/10.1088/0953-4075/31/10/014>.
- [7] Misha Yu Ivanov, Michael Spanner, and Olga Smirnova. “Anatomy of strong field ionization”. In: *Journal of Modern Optics* 52.2-3 (2005), pp. 165–184. DOI: 10.1080/0950034042000275360. URL: <https://doi.org/10.1080/0950034042000275360>.
- [8] N B Delone and Vladimir P Krainov. “Tunneling and barrier-suppression ionization of atoms and ions in a laser radiation field”. In: *Physics-Uspekhi* 41.5 (May 1998), p. 469. DOI: 10.1070/PU1998v041n05ABEH000393. URL: <https://dx.doi.org/10.1070/PU1998v041n05ABEH000393>.
- [9] Kenichi L. Ishikawa. “High-Harmonic Generation”. In: *Advances in Solid State Lasers*. Ed. by Mikhail Grishin. Rijeka: IntechOpen, 2010. Chap. 19. DOI: 10.5772/7961. URL: <https://doi.org/10.5772/7961>.
- [10] B. Bezzerides, R. D. Jones, and D. W. Forslund. “Plasma Mechanism for Ultraviolet Harmonic Radiation Due to Intense CO₂ Light”. In: *Phys. Rev. Lett.* 49 (3 July 1982), pp. 202–205. DOI: 10.1103/PhysRevLett.49.202. URL: <https://link.aps.org/doi/10.1103/PhysRevLett.49.202>.
- [11] Dietrich von der Linde and Kazimierz Rzazewski. “High-order optical harmonic generation from solid surfaces”. In: *Applied Physics B* 63 (Oct. 1996), pp. 499–506. DOI: 10.1007/s003400050115.
- [12] Luis Plaja et al. “Generation of attosecond pulse trains during the reflection of a very intense laser on a solid surface”. In: *J. Opt. Soc. Am. B* 15.7 (July 1998), pp. 1904–1911. DOI: 10.1364/JOSAB.15.001904. URL: <https://opg.optica.org/josab/abstract.cfm?URI=josab-15-7-1904>.
- [13] Teodora Baeva, S Gordienko, and A. Pukhov. “Theory of high-order harmonic generation in relativistic laser interaction with overdense plasma”. In: *Physical review. E, Statistical, nonlinear, and soft matter physics* 74 (Oct. 2006), p. 046404. DOI: 10.1103/PhysRevE.74.046404.
- [14] S. Gordienko et al. “Relativistic Doppler Effect: Universal Spectra and Zeptosecond Pulses”. In: *Phys. Rev. Lett.* 93 (11 Sept. 2004), p. 115002. DOI: 10.1103/PhysRevLett.93.115002. URL: <https://link.aps.org/doi/10.1103/PhysRevLett.93.115002>.
- [15] T D Arber et al. “Contemporary particle-in-cell approach to laser-plasma modelling”. In: *Plasma Physics and Controlled Fusion* 57.11 (Sept. 2015), p. 113001. DOI: 10.1088/0741-3335/57/11/113001. URL: <https://dx.doi.org/10.1088/0741-3335/57/11/113001>.
- [16] F. F. Chen. *Introduction to plasma physics*. New York: Plenum Press, 1974.
- [17] The Manim Community Developers. *Manim - Mathematical Animation Framework*. Version v0.17.3. Apr. 2023. URL: <https://www.manim.community/>.

- [18] Alin Suciu et al. “Parallel implementation of a PIC simulation algorithm using OpenMP”. In: Sept. 2020, pp. 381–385. DOI: 10.15439/2020F130.
- [19] A. Bourdier. “Oblique incidence of a strong electromagnetic wave on a cold inhomogeneous electron plasma. Relativistic effects”. In: *The Physics of Fluids* 26.7 (1983), pp. 1804–1807. DOI: 10.1063/1.864355. URL: <https://aip.scitation.org/doi/abs/10.1063/1.864355>.
- [20] J. D. Hunter. “Matplotlib: A 2D graphics environment”. In: *Computing in Science & Engineering* 9.3 (2007), pp. 90–95. DOI: 10.1109/MCSE.2007.55.
- [21] Charles R. Harris et al. “Array programming with NumPy”. In: *Nature* 585.7825 (Sept. 2020), pp. 357–362. DOI: 10.1038/s41586-020-2649-2. URL: <https://doi.org/10.1038/s41586-020-2649-2>.
- [22] Pauli Virtanen et al. “SciPy 1.0: Fundamental Algorithms for Scientific Computing in Python”. In: *Nature Methods* 17 (2020), pp. 261–272. DOI: 10.1038/s41592-019-0686-2.